Pergamon

Journal of Structural Geology, Vol. 16, No. 2, pp. 223 to 235, 1994

0191–8141/94 $06.00+0.00

The Maladeta granite polydiapir, Spanish Pyrenees: a detailed magneto-structural study

D. LEBLANC, G. GLEIZES, P. LESPINASSE, PH. OLIVIER and J.-L. BOUCHEZ

Laboratoire de Pétrophysique et Tectonique (URA 67 du CNRS), Université Paul-Sabatier, 38 rue des Trente-Six-Ponts, 31400 Toulouse, France

(*Received* 25 *June* 1992; *accepted in revised form* 30 *March* 1993)

Abstract—The Maladeta granitic complex (Spanish Central Pyrenees) has been subjected to a detailed magneto-structural study, through the systematic measurement of magnetic susceptibility and anisotropy of magnetic susceptibility at 253 regularly spaced sampling sites. Due to the dominant paramagnetic property of the granites, a first-order correlation can be derived between the susceptibility magnitude and the bulk-rock iron content, hence the petrographic nature of the rock. The Maladeta complex is shown to be composed of four principal juxtaposed plutons, each one being normally zoned, i.e. becoming more basic towards the periphery. The largest pluton, namely the Colomers unit, is itself made of a number of sub-plutons due to distinct but more-or-less coeval batches of magmas. The various magnetic data, complemented by field and microstructural observations, allow us to propose that the Maladeta polydiapir probably exploited NE- and SE-trending openings of the brittle crust for its emplacement, that accompanied or just preceded a SW-verging compressive event. A later N–S compression marked by inverse dextral, and E–W-trending shears, is preferably attributed to late Variscan rather than to Alpine tectonics.

INTRODUCTION

IN A STUDY concerning a mountain belt that results from superimposed tectonic events, such as the case of the Pyrenees, there are always difficulties in correctly attributing the respective kinematics of each event, namely the Variscan and Alpine events in the present case. In this respect, granite bodies can be most useful in recording events that are strictly related to their emplacement, by their magmatic foliation and lineation patterns. This magmatic record corresponds to a very short time interval when compared to the whole tectonic history of the belt. In addition, granites are very hard to imprint after their crystallization and, if imprinted by some deformation in the solid-state, it is quite easy to recognize the microstructural and structural signatures (high- or low-temperature deformation, direction and sense of shear). This contrasts with the country-rocks which usually best record the latest event.

The magmatic structures of granites however, are difficult to measure directly in the field or using classical measurement in the laboratory, even in thin sections. The techniques of low-field magnetic susceptibility (MS) and anisotropy of magnetic susceptibility (AMS) permit very accurate and less time-consuming measurements to be made, and also provide additional data which are helpful, for instance, in improving our knowledge on the rock-compositions and in quantifying the magmatic and/or solid-state strain. For this reason, the AMS technique has been systematically applied for some years to the study of Variscan granitoids in the Pyrenees (Bouchez *et al.* 1990, Gleizes *et al.* 1991), of which the Maladeta granite complex is an example. In our attempt to correlate the MS and AMS features with the field and microstructural information, we highlight the anatomy of a composite diapir, and show that three different kinematic stages can be unravelled in the Maladeta granite from its magmatic to its low-temperature states, and these stages probably have significance at the scale of the whole Pyrenean chain.

SETTING

The Maladeta granite massif is located in the Spanish part of the Central Pyrenees. It lies within the Axial Zone and, with an area of 400 km^2, it is one of the largest plutons in the orogen (Fig. 1). It was emplaced into country-rocks of Cambro-Ordovician to Carboniferous age, therefore at a shallow level of about 6 km in depth (Pouget *et al.* 1989). The country-rocks have been affected by very low-grade regional metamorphism together with a superimposed contact metamorphism aureole in which the sillimanite grade has been reached. The contacts between the granite and the country-rocks generally dip steeply northwards, both along the northern and southern borders of the pluton. These contacts are mostly undisturbed by post-magmatic tectonics. The pluton is considered to have been emplaced syn-tectonically (Evans 1992), but apparently rather late during the Variscan orogeny. The Permian age of some non-metamorphic rocks deposited on the northern part of the massif (Kleinsmiede 1960) is consistent with the rather young date of 277 ± 7 Ma (Rb/Sr; whole-rock) obtained for the granite by Vitrac-Michard *et al.* (1980). This date is representative of the cooling of the granite which, however, could be appreciably younger than emplacement (Pouget *et al.* 1989).

The Maladeta massif has principally been studied by Charlet (1968, 1979). This author defined a petrographic zoning in the western Aneto unit, with more basic rock-types surrounding the more acid, and indicated the

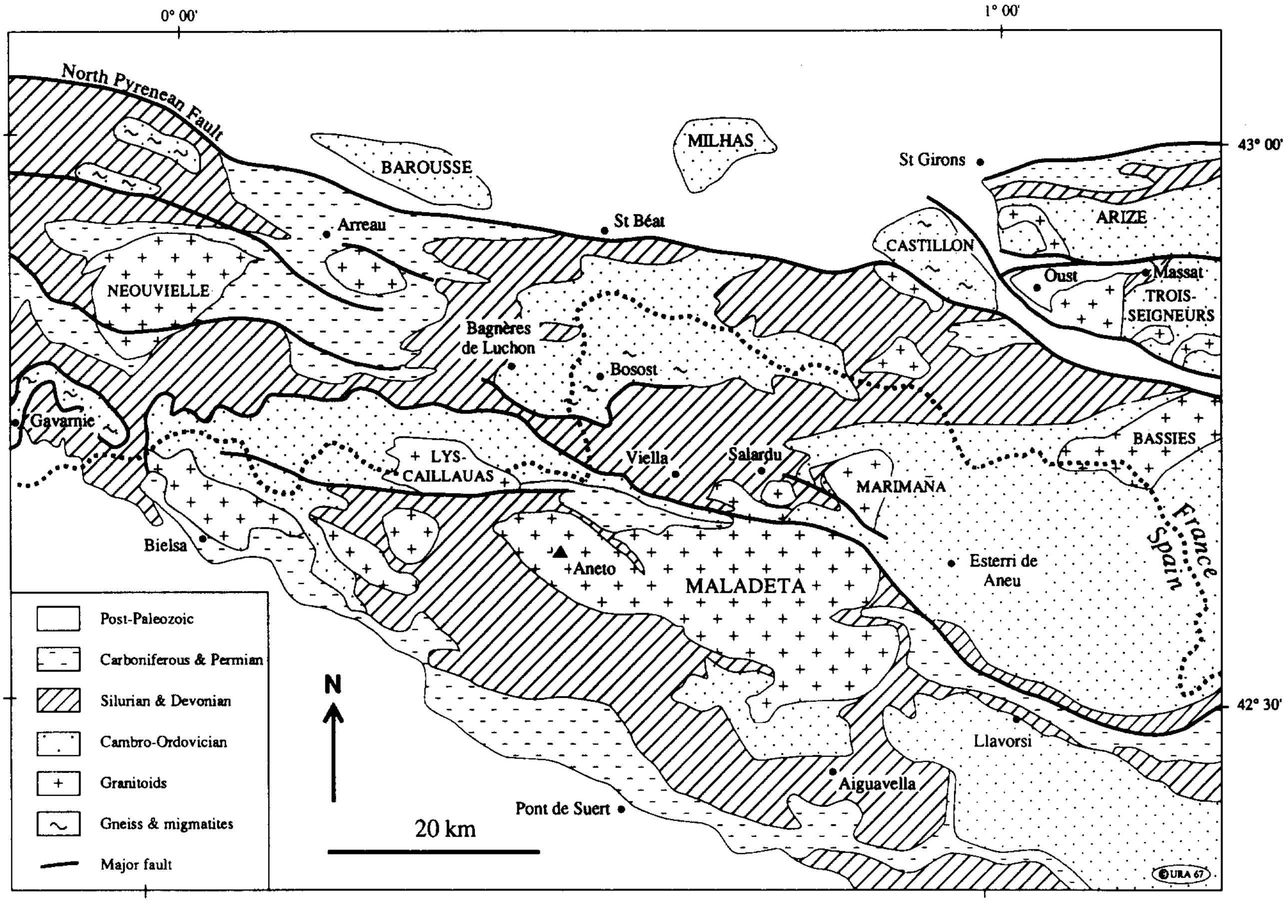

Fig. 1. Geological sketch map of the Central Pyrenees.

presence of gabbros in the Capdella unit, south-eastern part of the massif. He also noted that the granites are penetratively deformed in some places, particularly near the southern edge of the massif, and that major fault zones separate different units. He considered these faults, and the associated brittle to ductile deformation, to result from late Variscan tectonic events, but he admitted that reworking may have occurred during Alpine times. By contrast, Lamouroux (1991) considers these faults to be Alpine in age and sinistral in sense, associated with anti-clockwise rotations of the separate blocks.

RELEVANCE OF THE MS AND AMS STUDY

The relatively low MS magnitudes measured in the Maladeta complex indicate that the granites are dominantly paramagnetic, like similar Pyrenean granites where the lack of ferromagnetic minerals has been demonstrated (Gleizes *et al.* in press). In such paramagnetic granites, or ilmenite-type granites (Ishihara 1977), a linear correlation has been established between the low-field MS magnitude and the amount of iron in the rock, at least to a first approximation (Rochette 1987, Rochette *et al.* 1992). Iron is contained in the silicates, mainly biotite and amphibole, and is a significant component of the total composition of granitoids. Therefore, the knowledge of the iron content facilitates a mapping of the petrographic zoning of plutons (Gleizes *et al.* in press).

An AMS measurement is represented by the three principal axes $K_1 > K_2 > K_3$ of an ellipsoid. It has been progressively ascertained (King 1966, Rousset & Daly 1969, Guillet *et al.* 1983, Bouchez *et al.* 1990, Amice *et al.* 1991) that, when the rock structure is magmatic, the K_1 axis lies parallel to the magmatic lineation and the K_3 axis is perpendicular to the magmatic foliation.

The value of the AMS technique is increased by the possibility of quantifying the fabrics by calculating the total anisotropy, which is represented by the parameter $P_{\text{'para'}}\% = 100 \times [K_1 - D)/(K_3 - D) - 1]$ in which the diamagnetic contribution is substracted. The latter is considered to be constant and isotropic, and estimated as $D = -1.4 \times 10^{-5}$ SI (Hrouda 1986, Rochette 1987). The magnitude of the magnetic anisotropy is linked to the degree of preferred orientation of biotite (Launeau *et al.* 1990), normally the principal iron-bearing phase of our paramagnetic granites. Since the preferred orientation intensified with the shear strain (Ildefonse & Fernandez 1988, Ildefonse *et al.* 1992), AMS is a potential tool for the study of magma deformation during its emplacement. If a pluton has undergone subsequent deformation in the solid state, and this can be checked by microstructural observation in thin section, the intensity of that deformation might be estimated by the amount of reorientation of the AMS ellipsoid. The Flinn parameter also helps to characterize the shape of the

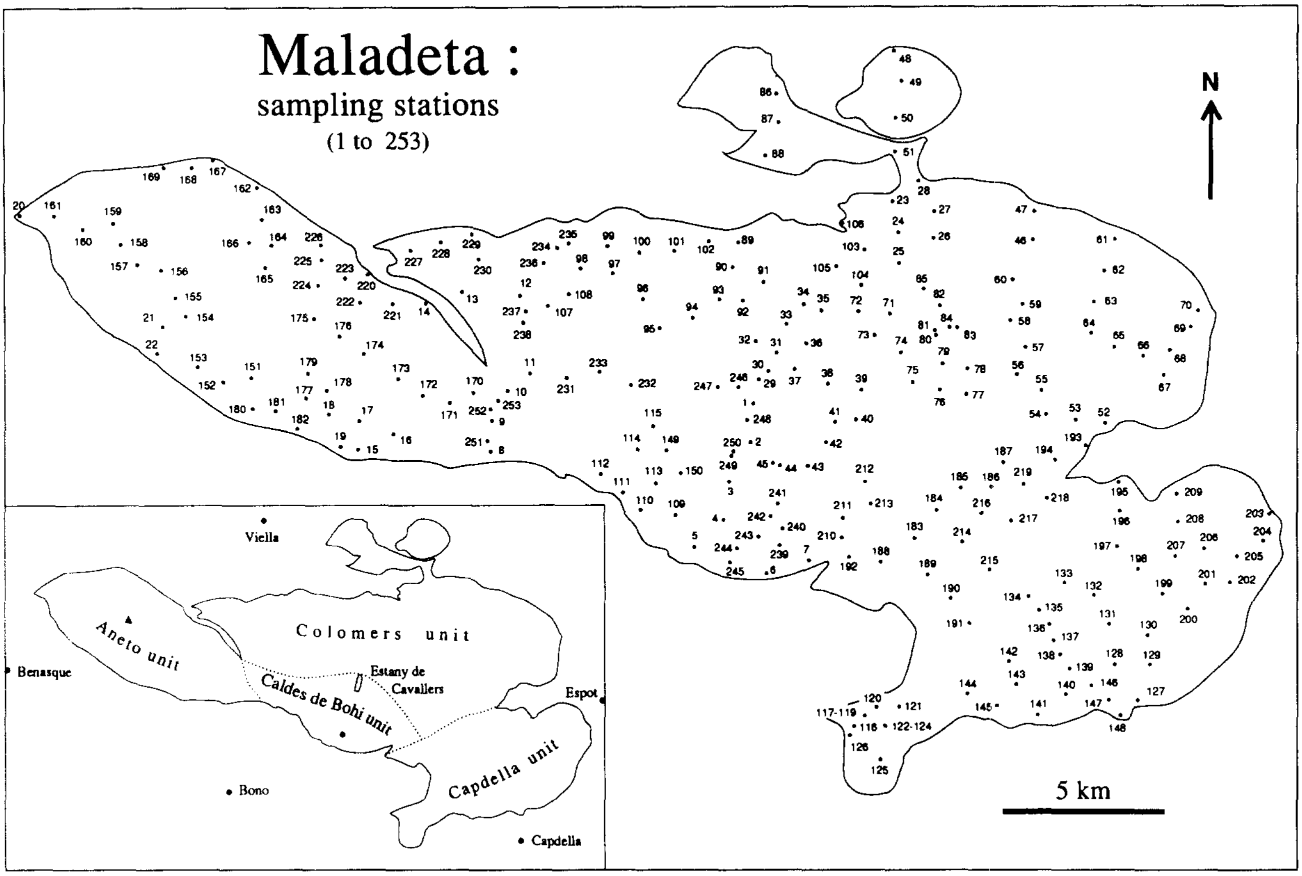

Fig. 2. Location of the sampling stations, and main units recognized in the present study in the Maladeta complex (inset).

ellipsoid of magnetic susceptibility. It is defined as $L - 1/F - 1$, L being the linear paramagnetic anisotropy $(K_1 - D)/(K_2 - D)$ and F the planar anisotropy $(K_2 - D)/(K_3 - D)$.

RELIABILITY OF THE MAGNETIC MEASUREMENTS

In the Maladeta complex, specimens were collected from 253 sites which were as regularly spaced as possible (Fig. 2). Two cores, a few metres apart, were drilled at every site and two specimens were cut from each core. The magnetic measurements were performed using the Kappabridge KLY 2 apparatus of Geofyzika Brno (Czechoslovakia) working at $\pm 3.8 \times 10^{-4}$ Tesla and 920 Hz. The values indicated in Table 1 are the mean values obtained from the four specimens recovered at each site, in the form of the arithmetic means for the MS and the eigen-vectors for the AMS.

A statistical study of our data (Fig. 3) has been performed to test the reliability of the MS values and AMS orientation data, and to evaluate the effects of anisotropy magnitude and shape of the magnetic ellipsoid on the within-site variabilities.

Within-site variability of the MS values

For each site (four specimens), we have calculated the mean susceptibility variation, in %:

$$V_K = 100(|K_a - K| + |K_b - |K| + |K_c - K| + K_d - K|)/4K$$

with K_a, K_b, K_c and K_d the susceptibility of each specimen, and K the average susceptibility of the site ($K = [K_a + K_b + K_c + K_d]/4$).

For the 253 sites, the average V_K equals 6.6%, and $V_K < 10\%$ is obtained for 85% of the sites (Fig. 3a). In the remaining 15% for which $V_K > 10\%$, the high V_K sometimes obviously results from a biotite-enriched enclave which was inadvertently incorporated in a specimen. The corresponding specimen, therefore considered as not representative of the site current rock-type, was discarded for the calculation of the site average MS value. We also observed that many of the high V_K were found for sites having either particularly high average susceptibility values ($K > 30 \times 10^{-5}$ SI) or very low values ($K < 10 \times 10^{-5}$ SI). This indicates that the corresponding rock-types have a rather heterogeneous distribution of their biotites, at least on the scale of the 43 cm^3 that form the sampling volume of a site. This

Table 1. MS and AMS data of the 253 sampling stations

N° site	K 10-5 SI	K1	K3	P para%	Flinn	N° site	K 10-5 SI	K1	K3	P para%	Flinn	N° site	K 10-5 SI	K1	K3	P para%	Flinn	N° site	K 10-5 SI	K1	K3	P para%	Flinn
1	23.9	249 / 37	129 / 34	1.7	2.4	65	18.6	83 / 42*	357 / 1	3.9	0.4	129	18.6	66 / 63*	320 / 3*	1.4	0.3	193	22.1	296 / 69	130 / 20	4.6	0.7
2	18.1*	145 / 4	50 / 58	3.1	0.8	66	17.5	37 / 37	135 / 5	2.2	1.4	130	17.6	59 / 60	328 / 1	1.4	0.5	194	20.4	61 / 38	157 / 7	2.2	0.4
3	24.6	307 / 9	212 / 30	4.4	1.0	67	21.2	10 / 9	99 / 15	1.6	0.4	131	15.2	203 / 34	326 / 26	1.9	0.6	195	19.4	20 / 18	251 / 66	2.3	1.3
4	27.0*	331 / 50	211 / 22	2.3	0.7	68	19.1	3 / 51	91 / 7	2.1	0.9	132	17.9	84 / 19*	260 / 79	1.9	0.7	196	17.1	286 / 30*	183 / 14	1.7	0.6
5	26.8*	312 / 58	194 / 15	5.5	0.9	69	22.0*	1 / 37	269 / 3	2.1	1.0	133	9.1	99 / 3	182 / 4	2.4	1.7	197	17.6	53 / 15*	330 / 66	2.3	0.7
6	24.2	87 / 8	185 / 35	5.2	0.4	70	23.7	162 / 35*	84 / 5	1.8	0.8	134	17.1	*	*	1.3	0.8	198	14.4	220 / 44*	313 / 44*	1.6	0.6
7	17.0	258 / 7*	350 / 17*	2.7	0.2	71	20.4	324 / 57	168 / 32	6.4	0.6	135	17.8	257 / 74*	351 / 2	2.5	0.8	199	17.1	*	337 / 39	1.8	1.3
8	44.6*	350 / 46	195 / 39	8.9	0.3	72	18.8	317 / 74	161 / 13	3.4	1.8	136	15.7	243 / 41*	24 / 38*	1.6	0.4	200	19.6	14 / 15	107 / 36	2.2	0.7
9	22.2*	175 / 66	13 / 21	5.3	0.2	73	16.7	324 / 32*	196 / 51	2.3	0.6	137	16.9	248 / 6	161 / 9	1.7	1.9	201	19.9	20 / 31	108 / 4	2,0	1.1
10	18.8	99 / 6	193 / 9	2.8	1.8	74	15.7	315 / 64	169 / 25	4.6	0.4	138	17.4	85 / 11*	344 / 16	2.3	0.7	202	20.3	11 / 29	127 / 31	1.5	1.2
11	24.3	158 / 14*	253 / 22*	5.3	0.3	75	7.7	30 / 1	122 / 18	3.9	1.2	139	21.1	61 / 15	163 / 38	1.2	0.7	203	23.3	349 / 40	92 / 12	1.4	2.2
12	20.0	16 / 74	273 / 7	2.7	2.1	76	16.9	208 / 61	*	2.1	1.3	140	19.2	2 / 10	155 / 73*	1.6	1.1	204	22.1	355 / 77*	81 / 2	1.4	0.6
13	25.0	331 / 39	196 / 41	1.7	0.5	77	6.3	213 / 40	16 / 48	4.9	0.9	141	20.1	241 / 17*	86 / 73	1.5	0.8	205	19.8	341 / 42	84 / 12	1.7	1.0
14	33.0	343 / 68	219 / 13	5.3	0.2	78	13.7	23 / 37	242 / 52	2.3	0.9	142	19.5	263 / 23*	180 / 3	1.4	0.5	206	15.7	24 / 22*	281 / 22*	1.2	1.2
15	30.3	301 / 73	193 / 5	6.4	0.2	79	15.3	25 / 43	208 / 53	1.8	1.0	143	17.1	266 / 36	161 / 40	1.6	1.0	207	19.0	191 / 9	93 / 13	1.8	0.8
16	27.5	313 / 57	174 / 24	3.2	0.6	80	16.8	331 / 61	182 / 26	2.7	1.4	144	18.2	73 / 9	176 / 40	1.4	0.6	208	18.4	18 / 69	300 / 1	2.0	0.6
17	27.7*	341 / 58	187 / 31	3.6	0.3	81	16.2	11 / 66	145 / 17	3.6	1.0	145	20.9	263 / 0	168 / 76	1.3	0.7	209	20.1	235 / 57	130 / 8	1.6	2.8
18	28.8	285 / 54	157 / 24	3.9	0.2	82	19.7	18 / 30*	184 / 56*	2.6	1.0	146	17.8	256 / 20*	156 / 39*	1.8	0.5	210	22.0	344 / 16	238 / 31	6.7	0.4
19	28.1	309 / 63	194 / 13	6.1	0.2	83	17.2	305 / 48	195 / 18	5.8	0.5	147	19.6	276 / 47	159 / 25	2.0	0.5	211	16.4	57 / 57	182 / 19	2.4	0.5
20	53.7	312 / 51*	45 / 22*	2.5	0.9	84	18.9	325 / 70	173 / 18	3.7	0.8	148	27.8	32 / 23	171 / 68	1.8	1.7	212	23.5	249 / 46	1 / 19	4.1	0.2
21	17.8	135 / 12	44 / 3	4.6	0.4	85	19.1*	324 / 41*	88 / 18	1.5	1.2	149	18.6	311 / 66	217 / 2	6.3	0.3	213	31.5	245 / 12	113 / 74	4.8	0.3
22	29.6	316 / 46	213 / 12	3.5	0.2	86	11.5	315 / 55	51 / 3	3.6	2.3	150	17.5	333 / 43	174 / 45	6.3	0.8	214	21.6	342 / 65	111 / 15	4.0	0.9
23	19.1	244 / 4	339 / 51	2.1	0.3	87	12.4	338 / 66*	213 / 49*	4.2	0.6	151	17.6	273 / 8	160 / 81*	3.2	0.6	215	21.2	53 / 39	173 / 30	2.9	1.5
24	16.8	311 / 36	198 / 20	1.3	0.5	88	36.4	138 / 20	6 / 64	1.7	0.7	152	28.4	60 / 52	186 / 27	4.5	0.3	216	16.1	8 / 77	163 / 16	5.2	0.6
25	18.7	289 / 59	161 / 24	1.9	0.4	89	23.6	345 / 58	188 / 29	6.2	0.4	153	28.2*	72 / 49	194 / 23*	4.8	0.2	217	17.6	55 / 53	237 / 38	3.3	2.1
26	19.6	211 / 73	336 / 9	3.9	1.2	90	22.2	304 / 3*	214 / 40	1.9	0.5	154	16.2*	281 / 12	16 / 17	1.9	0.5	218	19.3	8 / 41	183 / 49	3.4	0.8
27	19.2	209 / 57	32 / 34	2.1	1.0	91	17.8	351 / 41*	178 / 56*	1.3	1.8	155	16.5	176 / 57	56 / 17*	2.3	1.7	219	29.7	2 / 14	218 / 73	4.0	0.6
28	21.8	267 / 46	149 / 25	4.0	0.4	92	17.2	82 / 14	190 / 45	1.8	1.1	156	19.4	353 / 7	102 / 71	3.5	0.9	220	36.4	346 / 71	226 / 7	2.9	1.3
29	17.5	50 / 14	154 / 47	2.5	0.4	93	17.8	311 / 44*	199 / 22	2.1	0.3	157	18.3	329 / 53	99 / 26	4.3	0.2	221	18.7	319 / 33	222 / 10	3.1	0.8
30	16.2	317 / 22	78 / 50	2.6	0.2	94	18.0	73 / 31*	165 / 0	1.9	0.4	158	16.5	212 / 16	114 / 28	3.4	1.0	222	18.8	125 / 15	223 / 27	2.9	0.4
31	16.8	281 / 36	94 / 53	1.8	1.4	95	18.3	339 / 27	171 / 60	1.8	1.4	159	15.4	12 / 37	127 / 30	3.2	0.8	223	16.3	348 / 37	224 / 36	4.6	0.8
32	16.7	289 / 19	167 /59	2.3	0.7	96	17.7	132 / 11*	228 / 38	1.9	0.5	160	28.5	80 / 82	309 / 5	2.8	0.8	224	17.4	294 / 9	131 / 82*	2.6	0.7
33	15.3	*	286 / 6*	1.4	0.5	97	22.8*	291 / 26	169 / 47	1.6	0.8	161	34.8	345 / 2	253 / 27	2.4	0.5	225	21.6	5 / 34	220 / 49	2.7	0.6
34	16.1*	321 / 17*	355 / 46	2.9	0.4	98	21.8	284 / 23	181 / 28	4.1	0.2	162	33.9	95 / 49	206 / 18	2.2	0.3	226	30.3	312 / 55	197 / 16	3.2	1.3
35	19.6	290 / 34	153 / 47	1.4	0.9	99	22.3	262 / 15*	167 / 26	3.2	0.1	163	23.8	102 / 55	197 / 1	2.8	0.5	227	20.7	211 / 67	315 / 7	2.9	0.7
36	20.3	38 / 37	137 / 16	2.4	0.6	100	22.4	305 / 43	177 / 31	4.2	0.2	164	18.6*	314 / 39*	172 / 43*	2.3	0.1	228	20.4	253 / 60	134 / 15	5.9	0.4
37	16.0	311 / 9	47 / 38	2.6	2.4	101	22.2	311 / 63	190 / 13	4,0	0.6	165	17.9*	344 / 27	133 / 57	2.8	0.4	229	22.8	34 / 48	149 / 20	2.6	1.6
38	16.1	225 / 20	8 / 61*	5.1	0.6	102	21.2	322 / 78*	188 / 3	2.6	0.5	166	15.8	82 / 3	334 / 82	3.0	0.5	230	22.4	44 / 68	157 / 10	2.0	0.5
39	15.6	258 / 3	171 / 25*	1.4	0.5	103	7.8	325 / 3*	229 / 51	2.1	0.5	167	43.1	260 / 40	354 / 5	2.5	0.6	231	23.1	34 / 48	239 / 38	3.1	0.3
40	17.7*	72 / 2	196 / 83*	2.2	0.9	104	15.8	310 / 41*	171 / 43*	1.8	0.9	168	29.4	292 / 70	178 / 8	1.9	0.4	232	15.6	77 / 20*	15 / 1	1.3	1.3
41	17.3*	48 / 10	288 / 70	8.5	0.3	105	17.1	31 / 66*	254 / 28	1.8	0.9	169	29.4	276 / 13	179 / 29	2.7	0.2	233	19.0	27 / 49	237 / 33	2.5	1.4
42	27.1	187 / 41	8 / 49	7.8	0.1	106	21.4*	322 / 70*	202 / 10	5.3	0.2	170	19.7	249 / 42	94 / 44	3.2	0.3	234	24.3	300 / 41	141 / 48	2.9	0.3
43	19.1	223 / 7	358 / 76*	1.4	0.9	107	21.8	73 / 66*	322 / 8	2,0	0.3	171	19.8	238 / 25	340 / 24	3.6	1.5	235	25.1	276 / 40	151 / 35	3.9	0.2
44	12.1	277 / 28	359 / 17	2.6	0.6	108	23.7	223 / 36	326 / 19*	1.3	1.0	172	19.9	246 / 5	10 / 82	4.9	0.9	236	20.6	353 / 58	156 / 28	3.3	0.3
45	4.0	106 / 20*	0 / 53	2.6	0.4	109	26.1	318 / 68	189 / 22	2.5	0.8	173	18.4	242 / 15	341 / 32	4.3	1.2	237	23.0	51 / 72	303 / 5	2.0	1.5
46	19.7	83 / 63	191 / 9	4.0	0.9	110	24.1	140 / 73	35 / 6	3.3	1.0	174	16.9*	87 / 43	324 / 30	3.8	1.5	238	24.7	41 / 44	261 / 34	1.7	1.1
47	21.2	140 / 13	32 / 53	2.3	0.3	111	21.1*	335 / 72*	222 / 16*	2.2	0.8	175	17.4*	110 / 4	194 / 2	4.1	0.5	239	22.0	116 / 26	231 / 43	3.9	0.2
48	28.1	339 / 55*	165 / 38	1.1	0.2	112	27.4	258 / 59	129 / 20	4.1	0.4	176	16.2	279 / 53	119 / 36	2.4	1.2	240	12.4	149 / 46	47 / 19	2.5	1.1
49	23.5	344 / 42	175 / 47	3.3	0.2	113	21.5	323 / 5	224 / 33	2.9	1.2	177	14.8	242 / 58*	6 / 16	4.2	0.4	241	17.3	334 / 10	233 / 40	2.2	0.6
50	31.0	326 / 69	179 / 18	5.8	0.5	114	18.3	155 / 9	255 / 72	2.9	0.9	178	17.9	83 / 42	351 / 1	2.8	1.2	242	17.9	130 / 23	287 / 65	5.8	0.5
51	25.9	349 / 59	189 / 29	5.1	1.1	115	19.7	335 / 12	72 / 22	3.3	0.5	179	18.6	217 / 62	2 / 25	3.9	1.7	243	676	135 / 25*	31 / 6*	15.1	0.5
52	26.2	299 / 47*	138 / 48	2.3	1.0	116	47.9	26 / 38	226 / 51	3.2	0.4	180	27.3	41 / 60	173 / 21	2.1	0.4	244	29.1*	148 / 11	240 / 7*	3.9	2.1
53	20.9	264 / 54	116 / 25*	1.8	0.8	117	37.4	297 / 72	39 / 5	2,0	0.6	181	27.8	69 / 61*	185 / 5	5.5	0.3	245	20.9	106 / 17*	222 / 49	3.7	0.3
54	18.4*	290 / 61	183 / 10	5.6	0.2	118	28.7	94 / 65	333 / 16	0.8	1.1	182	27.1	71 / 71	187 / 9	7.2	0.2	246	17.5	248 / 11	11 / 65	8.1	0.5
55	18.1	351 / 41	189 / 47	4.3	0.6	119	25.2	96 / 69	284 / 21*	1.6	0.5	183	28.5*	18 / 33	139 / 37	8.2	1.7	247	17.2	272 / 5	6 / 60	4.7	0.3
56	17.5	295 / 1	204 / 11	1.8	1.0	120	21.3	130 / 79	293 / 9	2.2	1.0	184	22.5	317 / 16	88 / 64	2.9	0.4	248	18.6	285 / 2	183 / 71	2.4	0.7
57	18.6	254 / 56	171 / 3	1.8	1.1	121	20.5	221 / 77	106 / 0	1.8	1.3	185	6.1	15 / 44	159 / 40	3.6	0.6	249	19.8	123 / 2*	25 / 69	4.8	0.2
58	16.5	38 / 30*	154 / 36	2.0	0.6	122	33.4	336 / 65*	142 / 10*	1.5	0.6	186	20.6	3 / 51	168 / 38	5.4	0.3	250	0.7	138 / 32*	1 / 52	3.0	0.5
59	16.0	19 / 54	163 / 31	1.7	1.2	123	40.1	115 / 29	264 / 58	1.2	0.8	187	16.5	13 / 11	110 / 31	6.6	0.5	251	30.7*	13 / 35*	204 / 53	4.9	0.3
60	18.8	170 / 47	355 / 40	1.4	1.5	124	43.8	41 / 61	188 / 19	1.3	0.6	188	25.5	23 / 47	218 / 42	3.5	0.7	252	31.6	68 / 26	318 / 37	9.8	0.4
61	26.4	119 / 28	20 / 10	2.2	0.8	125	62.1	46 / 37	207 / 58	1.6	0.9	189	20.5	52 / 58	223 / 30	3.4	0.5	253	17.9	219 / 31	118 / 17	3.6	1.0
62	18.1	280 / 13*	192 / 28	2.0	0.7	126	36.5	138 / 23	241 / 28	1.2	0.7	190	17.6*	60 / 4	334 / 21	1.6	0.6						
63	14.6	80 / 9	175 / 39	1.6	1.1	127	20.3	37 / 20	145 / 37	1.9	0.9	191	18.3	208 / 36	309 / 21	1.6	0.8						
64	19.6	66 / 38*	246 / 52	1.9	0.9	128	19.1	37 / 42	132 / 4	1.4	0.8	192	27.9	63 / 31	195 / 51	4.0	0.4						

K = magnitude of the magnetic susceptibility; K_1 = azimuth and plunge of the magnetic lineation (in degrees); K_3 = azimuth and plunge of the pole of the magnetic foliation; $P_{para}\%$ = anisotropy magnitude; Flinn = Flinn parameter.
*Indicates a poorly constrained value or a discarded, non-significant, measurement.

heterogeneity is attributable to grain-size in the low-susceptibility rocks and to short-range variations in the partition between the felsic and the mafic fractions in the high-susceptibility rocks. The relatively high V_K values of these rocks do not impede, generally, their assignment to the susceptibility classes into which they have been sorted. There remains, however, about 10% of the sites (starred in Table 1) with $V_K > 10\%$, for which we admit that our sampling is not fully representative of the site MS magnitude.

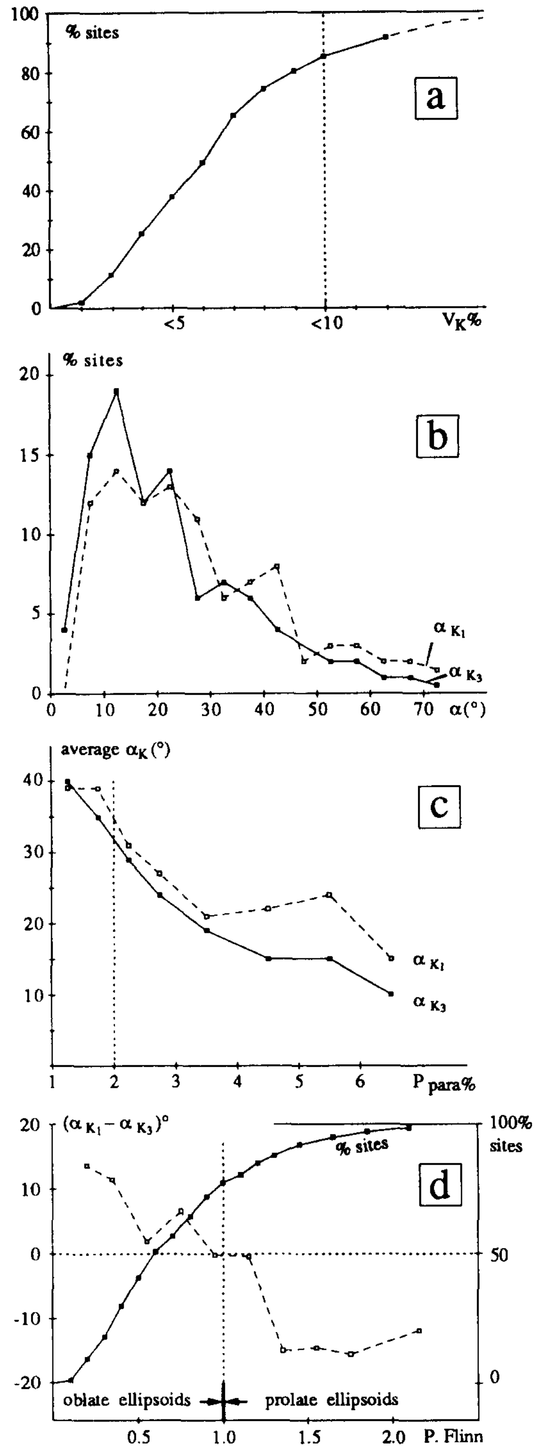

Fig. 3. Within-site variabilities of the magnetic measurements. (a) Variability of the susceptibility magnitude: cumulative frequency of sites vs V_K% (see text); (b) variability of the orientation measurements: frequency of sites vs αK_1 (broken line) and αK_3 (see text); (c) role of total anisotropy on directional variability: average αK for a given value of $P_{\text{'para'}}$%; (d) role of the shape of the magnetic ellipsoids: ($\alpha K_1 - \alpha K_3$) vs the Flinn parameter (broken line) and cumulative frequency of sites vs P_{Flinn}.

Within-site variability of the orientation data

Because of the small number of specimens at each site, a sophisticated analysis of the statistics on the orientations would not be realistic. Instead, within-site variability will be examined using αK_1 (and αK_3) defined as the maximum angular departure between the mean direction of K_1 (respectively K_3), and the directions of individual K_1 (respectively K_3) of the four specimens of the site.

$\alpha K_1 < 35°$ is observed for 68% of the sites, and $\alpha K_3 < 35°$ for 77% (Fig. 3b). Compilation on the whole massif leads us to consider that, up to this value of 35°, the tensor mean orientation of K_1 (respectively K_3) is a correct representation of the 'true' magnetic fabric. Among the remaining sites for which $\alpha > 35°$, a number are represented by three specimens with highly consistent orientations, while the fourth specimen departs greatly from the others. For these sites, the mean K_1 (and/or K_3) has been calculated from the three consistent specimens. αK recalculated from these specimens is frequently less than 20° and $\alpha K_1 < 35°$ is now obtained from 78% of the sites and $\alpha K_3 < 35\%$ from 87%. Admittedly, less confidence should be given to the remaining sites (starred in Table 1) for which $\alpha K > 35°$.

The relatively strong influence of the strength of the fabric on the within-site variability of the orientation data is examined in Fig. 3(c), plotting total anisotropy vs αK. For example, sites with $P_{\text{'para'}}\% < 2$ have an average αK larger than 30°, and the lowest αK values clearly correspond to the highest anisotropies.

The diagram of ($\alpha K_1 - \alpha K_3$) vs the Flinn parameter (Fig. 3d) stresses that K_3 is better defined than K_1 ($\alpha K_1 - \alpha K_3 > 0°$) for oblate magnetic ellipsoids ($P_{\text{Flinn}} < 1$), and K_1 is better defined than K_3 ($\alpha K_1 - \alpha K_3 < 0°$) for prolate ellipsoids ($P_{\text{Flinn}} > 1$). In fact, K_1 and K_3 are nearly equally defined if $0.5 \leq P_{\text{Flinn}} \leq 1.2$. K_3 being more often better defined than K_1 is also correlated with oblateness of the magnetic ellipsoid being more frequent than prolateness.

Lastly, it is worth noting that, even in sites where the orientation variability is high, the mean trends of the magnetic fabrics are still generally consistent, in map view, with those of the neighbouring sites. The Capdella unit (southeast of the massif) exemplifies this feature. Its low anisotropy, usually less than 2% (Fig. 6b), correlates with high within-site variabilities of its orientations (Fig. 3c), which does not preclude, however, the fact that lineations and foliations trend very consistently over the whole unit (Figs. 4 and 5).

MAGNETIC SUSCEPTIBILITY AND PETROGRAPHIC ZONING

The magnitudes of the magnetic susceptibility measured in the Maladeta complex range from $K = 4.0 \times 10^{-5}$ SI to $K = 62.1 \times 10^{-5}$ SI (Table 1). These values are typical of dominantly paramagnetic granites having Fe^{2+} (equivalent) wt % in the range of 0.8–9.5% (Gleizes *et al.* in press). Two exceptions are worth noting, namely site No. 250 corresponds to a fine-grained and highly leucocratic vein that gave an extremely low value of the MS ($K = 0.7 \times 10^{-5}$ SI), and

No. 243 in which the unexpectedly high value of the MS ($K = 676 \times 10^{-5}$ SI) is attributed to the occurrence of ferromagnetic grains.

The following correlations between the mean susceptibilities and the petrographic types have been established, based on microscopic examinations and rapid modal analyses of 145 specimens, using thin sections made from the same cores as used for the MS and AMS measurements (K in 10^{-5} SI):

$$K < 10 \text{ : leucogranites}$$
$$10 < K < 20 \text{ : monzogranites}$$
$$20 < K < 30 \text{ : granodiorites}$$
$$K > 30 \text{ : tonalites or gabbros.}$$

Note that the same correlations, with a few minor differences, have also been recognized in other granites of the Pyrenees (Gleizes *et al.* 1991, in press).

In map view (Fig. 6a), the MS magnitudes display a complex zoning that may be subdivided into several juxtaposed units.

(i) The *Aneto unit* in the west, despite a relative lack of samples in its centre due to difficult accessibility, reveals a regular petrographic zoning already recognized by Charlet (1968). Tonalitic rocks at the periphery grade inwards to biotite- and amphibole-bearing granodiorites. The core of the Aneto unit comprises monzogranites with biotite and muscovite. Note that the cordierite-bearing subtype identified by Charlet (1968) has not been observed. The transition between granodiorites and monzogranites is marked by a progressive but rapid decrease in susceptibility from 27×10^{-5} to 20×10^{-5} SI, achieved within a few tens of metres.

In the eastern part of the Maladeta complex, the distribution of susceptibility magnitudes allows us to identify three other units.

(ii) In the southeast, the *Capdella unit* (Fig. 2, inset) essentially comprises biotite- and amphibole-bearing granodiorites, and includes gabbros in its southwestern extremity. The granodiorites surround a core of monzogranites which, unlike in the Aneto unit, contain some amphibole in addition to biotite, but no muscovite. The transition from granodiorite to monzogranite is smooth and progressive. In contrast, the granodiorite–gabbro contact is rather abrupt, with a transition zone a few tens of metres wide where magma mingling with numerous enclaves of both rock-types within each rock-type is observed.

(iii) In the southern central part of the massif, the *Caldes de Bohi unit* is petrographically similar to the Aneto unit, except that tonalites are not represented.

(iv) In the north, the *Colomers unit* is by far the most complex unit with no regular zoning. It comprises granodiorites and monzogranites that everywhere contain biotite and accessory amphibole, except in the south near its contact with the Capdella unit, where amphibole is lacking and muscovite is present in addition to biotite.

Finally, leucogranitic bodies clearly cross-cutting all the other rock-types, and forming small intrusions or veins, occur in all units.

DATA FROM AMS

Orientation data

The map of *magnetic foliation* trajectories (Fig. 4), obtained by simple extrapolation of the foliation trace at each site, clearly identifies the Aneto unit to the west, the Capdella unit to the south, and a large and composite unit in the centre of the massif. Complemented by the magnetic susceptibility zonation (Fig. 6a), the latter is revealed as a super-unit comprising a southern unit (Caldes de Bohi) and a northern unit (Colomers), itself formed by the juxtaposition of three smaller bodies. The southernmost body comprises a muscovite-bearing monzogranite, contrasting with the two other bodies where monzogranites are amphibole-bearing. All these units or subunits (bodies) are characterized by foliation trajectories that are concentric, and that become nearly parallel to the contacts when approaching the country-rocks. However, foliations may be clearly oblique to the contact in some places on the northern border of the massif. Oblique-to-contact foliations are also observed in the gabbros in the south-west of the Capdella unit.

In the whole Maladeta massif, the foliations are mainly steeply dipping, generally with outward dips defining domes around each plutonic body. The Caldes de Bohi unit is, however, an exception with its inward dipping foliations.

In map view, the long axes of the plutonic bodies trend from ENE–WSW in the Capdella unit to WNW–ESE in the Aneto unit. In the latter, the mean foliation plane trends N97°E (Fig. 4: orientation diagram), i.e. obliquely to the elongation of the dome. To the south of the Aneto unit, the foliations are characterized by their opposite and convergent dips on both sides of a separation line (Fig. 4: grey broken line) which is about 1 km north of the contact with the country-rocks. This separation line is also apparent in the map of *magnetic lineations* (Fig. 5).

In general, the lineations are gently or moderately plunging over the whole massif. Their mean trends (Fig. 5: diagrams) are very different in the Capdella unit (N43°E) and in the Aneto unit (N316°E), emphasizing the strong structural contrast between these units. The detailed orientation distribution of the two types of lineations is, however, somewhat complex. The lineations mostly have consistent trends in the inner parts of the Caldes de Bohi and Capdella units but are rather scattered in their peripheries. In the Colomers unit the lineations trend more or less conformably with the Aneto lineations or the Capdella lineations. At the boundary between the Colomers and the Capdella units, the Rio de Sant Nicolau area (Fig. 5: stippled) has lineations with homogeneous trends to the north (mean trend 7°N43°), strongly contrasting with the lineation patterns occurring further north and south.

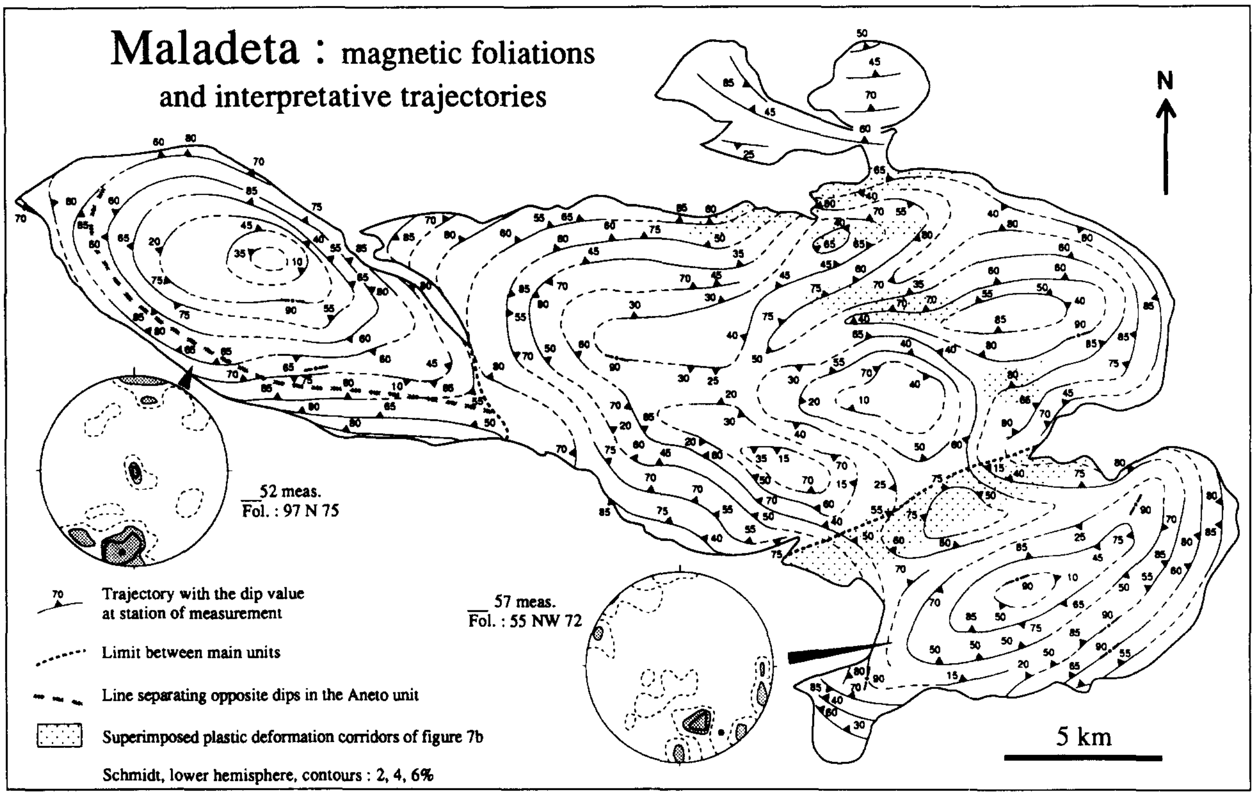

Fig. 4. Magnetic foliations with interpretative trajectories, and orientation diagrams for the Aneto and Capdella units.

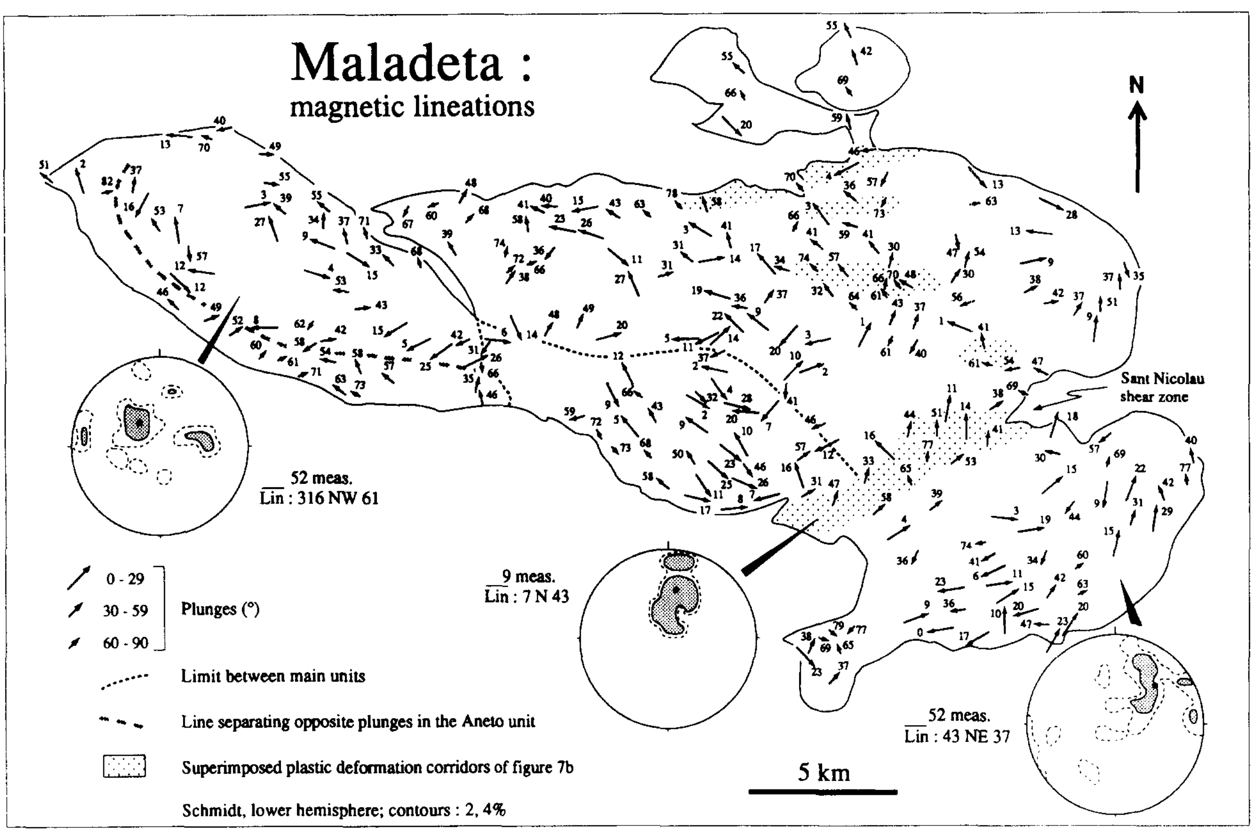

Fig. 5. Magnetic lineations, and orientation diagrams for the Aneto unit, Capdella unit and Sant Nicolau shear zone.

Scalar data

In the Maladeta complex, the *total anisotropy* parameter P'_{para}, ranges from 0.8 to 9.8%. Map of the anisotropy isovalues (Fig. 6b) emphasizes that the high anisotropy zones are organized into strips with two main orientations, namely N70°E and N110°E. These are observed principally at the borders of plutons, either close to contacts with the country-rocks (south of the Caldes de Bohi unit, south and east of the Aneto unit), or at contacts between plutons, namely between the Capdella and Colomers units, and between the Caldes de Bohi and both the Colomers and Aneto units. High anisotropies (>5%) are also recorded locally within plutons, particularly in the core of the Caldes de Bohi unit and, in places, within the Colomers unit. In contrast, typically low anisotropies (<2%) are principally recorded in the Capdella unit and in the core of the Colomers unit.

In order to improve our constraints on the contact zone between the Caldes de Bohi unit and the Colomers unit, a relatively dense sampling has been performed along the Estany de Cavallers traverse (Fig. 2, inset). The data highlight the abrupt juxtaposition of a very anisotropic zone with an almost isotropic zone (Fig. 6b). Taking the susceptibility data (Fig. 6a) into account and allowing for a normal petrographic zoning in each pluton, we conclude that the highly anisotropic zone belongs entirely to the Colomers unit.

The map of the *Flinn parameter* (Fig. 7a) underlines a very strong correlation between the areas of highest anisotropy and the most planar zones. In contrast, areas with a linear fabric generally coincide with the cores of plutonic units where there is least anisotropy.

MICROSTRUCTURES

With respect to their microstructures, the granites of the Maladeta complex can be divided into three classes (Fig. 7b).

Class 1 *microstructures* characterize rocks with a strictly magmatic texture. Virtually no plastic deformation has affected the rock as indicated by quartz grains having only undulose extinctions or a few subgrain boundaries. Most of the Maladeta complex rocks belong to this class.

Class 2 *microstructures* correspond to rocks with a magmatic appearance in the field, but with evidence of some superimposed solid-state deformation when observed under the microscope. These rocks mostly show evidence of high-temperature plastic deformation features, such as kinked but stable biotite, and quartz grains replaced by subgrains with a mosaic pattern. Low-temperature deformation features may be present, marked by high-angle sub-boundaries and new grains of small size ($< 100\,\mu$m). Microfractures, that appeared at even lower temperatures as demonstrated by their infillings of quartz–chlorite–epidote ± calcite, may be superimposed on the latter features.

Where the low-temperature deformation intensifies and extends to the whole rock, the quartz grains become entirely recrystallized into a mosaic of new grains, and epidote becomes abundant, along with an increase of hydrothermal alteration, transforming plagioclase into sericite, and biotite into chlorite. At this stage a coarse gneissosity may appear in the rock.

Localities where a certain amount of strain in the solid-state is observed are frequently aligned in map view, and may be considered to belong to shear zones. In this respect, the Sant Nicolau area, south of the Colomers unit (Fig. 5), constitutes the most important shear zone of the Maladeta complex. Such alignments also affect the Colomers unit.

Class 3 *microstructures* occur in mylonitic bands where the intense solid-state deformation is easily recognized in the field. These rocks were not systematically collected for the AMS study but observations in thin section demonstrate that these bands, with their trends close to E–W and their northward dips, acted as reverse dextral faults, and therefore have a southward thrust component. Note that because they were not systematically mapped, these mylonitic bands are more numerous than actually reported on the map of Fig. 7(b).

DISCUSSION

Polydiapirism of the Maladeta complex

As emphasized by the map of the magnetic susceptibility isovalues (Fig. 6a), the petrographic zoning reveals a pattern actually composed of four main juxtaposed units. The Aneto and Caldes de Bohi units are similar: both are strongly anisotropic in their southern borders and much less so on their northern borders, and both display NW–SE-trending foliations and lineations. The Capdella unit is very different with low anisotropies everywhere, even on its borders, and with structural trends bending gradually from WSW–ENE to SSW–NNE (Fig. 5). The Colomers unit is more complex. Its northeastern part is comparable to Capdella for orientation and anisotropy. The remainder of the Colomers unit resembles the Aneto unit for structural orientation, but not for anisotropy, which is lower in the core and much higher on the northern border.

A common feature of all these units is a normal petrographic zoning, i.e. richer in iron away from the core and towards the periphery. However, the increase is not linear from core to periphery. Rather, the susceptibility magnitudes are arranged in zones with nearly constant values, and zones of steep gradients where the susceptibility increases abruptly. Such gradients are particularly obvious between granodiorites and gabbros in the Capdella unit, and between monzogranites and granodiorites in the Aneto unit. In the southern part of the Aneto unit, the steep gradient coincides exactly with the line along which lineations and foliations abruptly change their trends or dips (Figs. 4 and 5: grey broken line). A similar change is observed at the granodiorite-gabbro transition in the Capdella unit. Such a transition, where a change in both petrography (MS) and structure (AMS) is observed, constitutes evidence for the pluton to have been fed by separate magma batches differing in bulk composition, in viscosity and kinematic character, at a given time of the emplacement history. The same reasoning is valid for the clear-cut but magmatic contacts, along with the high susceptibility contrasts, between the small leucocratic stocks and their granitic host-rocks.

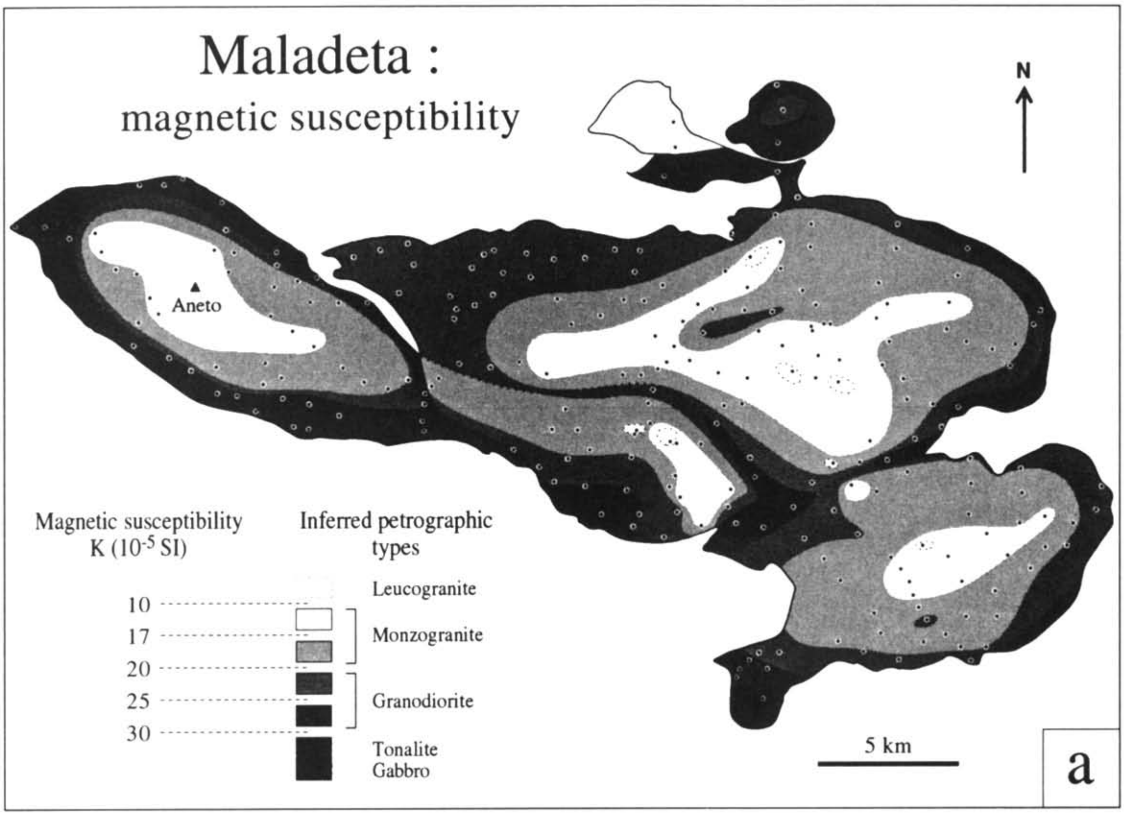

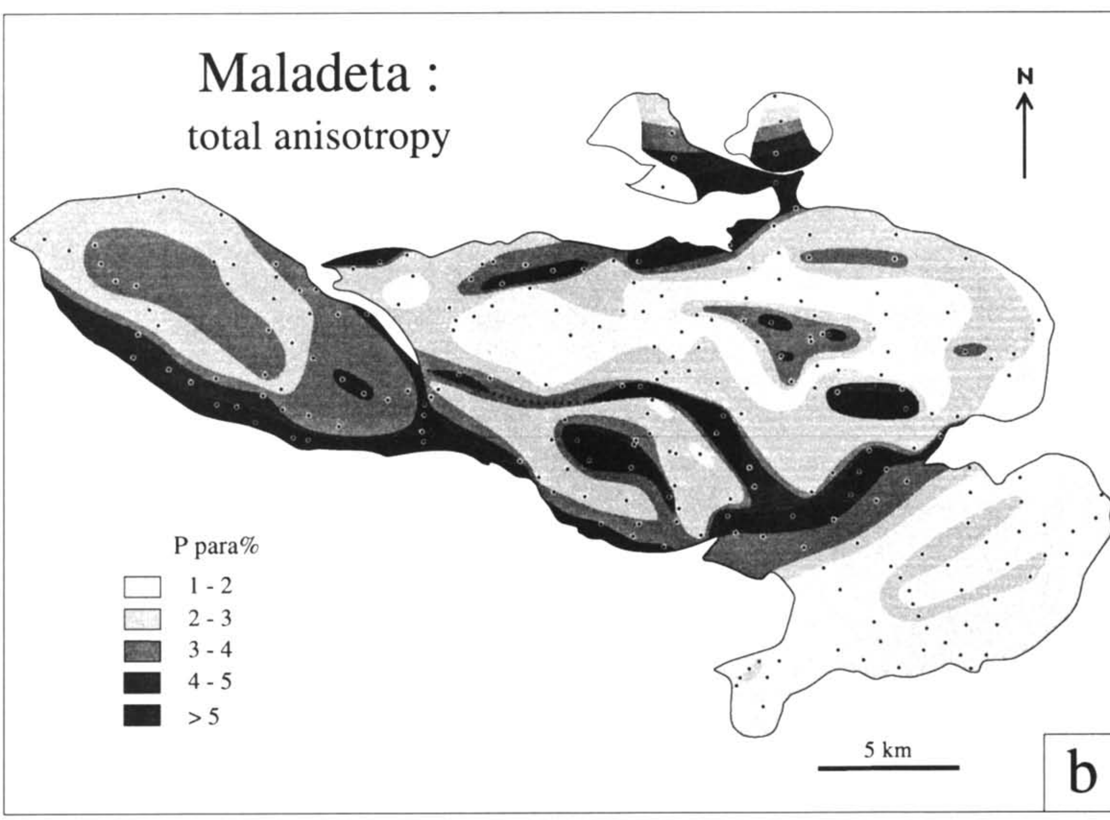

Fig. 6. (a) Magnetic susceptibility isovalues and inferred petrographic types; (b) total anisotropy isovalues.

The marked parallelism between the iso-susceptibility lines and the foliation trajectories, and their fine concentric arrangement, suggest that the individual plutons they define were progressively expanding perpendicularly to these lines, i.e. radially. The intrusion events may have been coeval in adjacent plutons, or successive in a given pluton. In a composite pluton, interferences between successive batches with different compositions may have occurred. This may explain the anomalies in the susceptibility zoning patterns of the Capdella and Colomers units.

The main trends, NE–SW and NW–SE, recorded in the Maladeta complex parallel to the mean lineation and foliation azimuths of the Capdella and Aneto units, respectively, may represent the opening directions in the crust which allowed the ascent of the magmas. The same structural trends have already been recorded in other Pyrenean granite massifs, like the Mont-Louis-Andorra pluton (Gleizes & Bouchez 1989). In this pluton, however, the NE–SW trend clearly pre-dates the NW–SE trend, in contrast with the Maladeta complex where the two families of orientations seem to be more or less coeval. The significance of this discrepancy remains unclear.

Deformation

Deformation features and fabrics within the three classes of microstructural states were examined and interpreted in terms of the history of the Maladeta complex.

Rocks with a magmatic microstructure (class 1). Their anisotropy results directly from the fabric of (mainly) biotite that was acquired through magma deformation during its late stage of emplacement before solidification. These rocks are usually the least anisotropic (1–3%) and slightly linear in fabric (Fig. 7a), but may be highly anisotropic (up to 8.6%) and strongly planar.

The highly anisotropic and planar zones describe elongated strips, generally oriented ESE (Fig. 6b) and located on the southern border of some units. This asymmetrical location is quite clear on the southern borders of the Aneto and Caldes de Bohi units, along their contacts with the country-rocks. A high anisotropy strip is also found between the Caldes de Bohi and Colomers units. As discussed earlier, this belongs to the southern fringe of the Colomers unit. The same type of asymmetrical pattern holds for the strip in the centre of the Caldes de Bohi unit, which marks the southern fringe of a monzogranitic body, itself separated from a more southerly granodiorite by a zone of abruptly increasing magnetic susceptibilities (Fig. 6a).

The cause of such a pattern of high anisotropy is not clear. It is noteworthy that the distribution of magnetic fabric intensities is sometimes closely linked to the distribution of petrographic compositions (compare maps of Figs. 6a & b). However, these two variables seem to be rather independent since, for instance, the tonalites in the margin of the Aneto unit (Fig. 6a) are highly anisotropic in the south and the east, but have particularly low anisotropies to the north (Fig. 6b). Hence, the intensity of fabric is thought to be related only to the amount of strain recorded by the magma during emplacement. The location of the anisotropic strips on the northern side of magmatic contacts could therefore imply that the 'northern' batch of magma was deforming against the 'southern', thus suggesting some viscosity contrast as well as some interval in time between successive batches. We think, however, that simple mechanical interactions between plutons, or bodies, during emplacement cannot solely account for the systematic increase of the degree of anisotropy along the southern borders of the magmatic bodies. This asymmetry, observed at the scale of the whole complex, allied to the overall tendency of the foliations to dip northwards, strongly suggest that some southward verging external tectonics was applied to the complex during emplacement.

Although not clearly related to a gradient in anisotropy magnitude, the converging lineation trajectories on both sides of the separation line in the southern Aneto (Fig. 5) might result from the interaction between the upwelling magma of this unit and the regional tectonics mentioned above. Whatever the origin of the pattern, the obliquity of these lineations with respect to the contact with the country-rocks demonstrates that, unlike the case of the Bassiès granite pluton (Gleizes *et al.* 1991), the high anisotropies do not result from a strike-slip displacement parallel to the contact.

Rocks with superimposed deformation in the solid-state (class 2). These are mainly found in corridors trending N75°E to N110°E (Fig. 7b), that roughly belong to the high anisotropy strips with planar fabrics already mentioned (Figs. 6b and 7a). Such corridors lie inside the Colomers unit. They seem to be related to close-to-solidus movements between bodies in this unit since their lineations, mostly moderately plunging to the northwest, do not significantly differ from those of the surrounding granites where microstructures are magmatic (Fig. 5). The Sant Nicolau area forms a km-wide corridor at the southern border of the Colomers unit. It is peculiar with its lineations regularly trending close to N–S (Fig. 5) which strongly contrast with those of their surroundings. The question of whether the Sant Nicolau corridor is related to the emplacement of the Maladeta complex, has to be examined.

Structural constraints at various scales in this corridor indicate that the overall geometry and fabrics resulted from deformations that were initiated in the magmatic state:

(i) foliation trajectories in the southern Colomers unit (Fig. 4) appear to be independent of the microstructural state of the Sant Nicolau corridor;

(ii) some sites display microstructures clearly retaining their high-temperature origin;

(iii) N–S-trending lineations have been observed at localities where either strong or weak deformation in the solid-state is observed;

(iv) in the corridor, the magnitude of anisotropy does not correlate with the intensity of the solid-state deformation.

These arguments strongly favour an interpretation for the formation of the Sant Nicolau corridor of a kinematic continuum, from the magmatic to the high-temperature solid-state. Adding the argument of constant orientation of the lineations of the corridor, we interpret the latter as forming a km-wide, ENE-trending shear zone that was initiated before the complete crystallization of the granite. Our data, however, do not constrain the sense of shear along the rather steeply

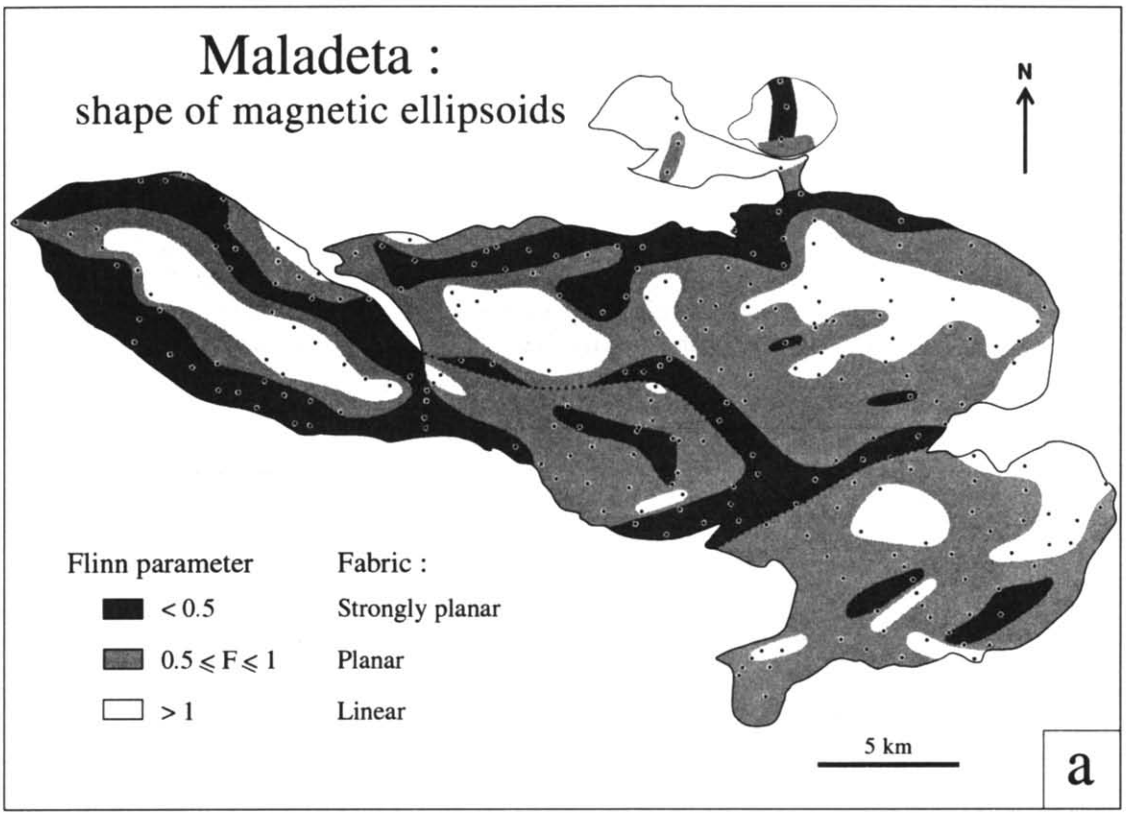

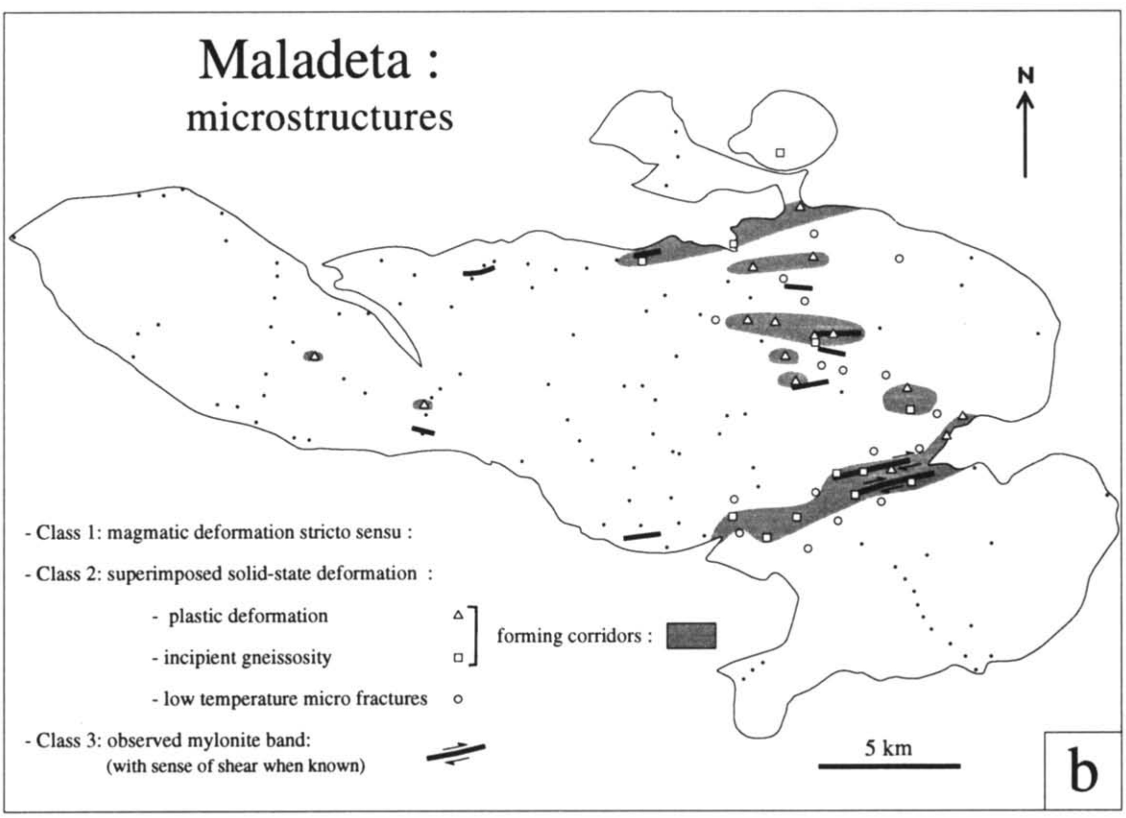

Fig. 7. (a) Flinn parameter isovalues and corresponding fabric types; (b) classes of microstructures in the Maladeta complex.

NNE-plunging lineations. Hence, either a thrust component to the southwest due to sinistral compression, or a dextral wrench related to an extensional event may be invoked.

Because high-temperature solid-state deformation occurred during the closing stages of emplacement of the Maladeta complex, this deformation probably resulted from the same state of stress as that which was responsible for the high anisotropy strips with planar fabrics separating some units or sub-units of the complex, and running along their southern borders. In the absence of definite evidence of shear sense in the granites, we conjecture that the tectonic regime that prevailed during emplacement was compressive, with a top-to-the-southwest thrust component, as suggested by Evans (1992) in his study of the immediate country rocks, south of the Aneto unit. A SW-verging thrust component would also be consistent with the overall steep northward dips of the granite foliations. This could account for the fact that the southern borders of the plutons suffered higher magmatic strains than those of the north.

The mylonitic bands. The Sant Nicolau corridor contains mylonitic rocks with foliations dipping steeply to the north (>60°), and lineations N330°E in mean azimuth. The kinematic indicators observed in oriented thin sections of these mylonites prove the bands to be dextral in map view. This sense of shear, and the resolved thrust component toward the southeast of these shear bands, are inconsistent with any of the mechanisms considered above for the Sant Nicolau penetrative deformation. Therefore, the mylonitic bands, that obviously formed later than the Sant Nicolau deformation because of their lower-temperature microstructures, must have resulted from a different regional stress regime. Note that, beyond the mylonites, the rocks imprinted by the low-temperature solid-state deformation retain their magmatic fabrics, as indicated by the fact that their AMS measurements do not differ from rocks having typically magmatic microstructures.

Finally, it is worth noting that dextral-inverse and roughly E–W-trending shear zones are widely recognized in the Pyrenees. The problem of their late Variscan (Carreras *et al.* 1980) or Alpine age (Lamouroux *et al.* 1980, Lamouroux 1991) is not solved (Soliva *et al.* 1991) even if direct dating attempts have given Alpine ages (McCaig & Miller 1986, Majoor 1988). The study of the Mont-Louis-Andorra pluton (Gleizes & Bouchez 1989) and general considerations on the scale of the whole Pyrenees (Gleizes *et al.* 1992), lead us to favour a late Variscan age for these compressional and dextral shears.

CONCLUSION

This AMS study has considerably increased the available constraints on the internal composition, emplacement and structural evolution of the Maladeta complex. The overall concentric and normal compositional zoning that was previously described in the western Aneto pluton (Charlet 1968), was unknown elsewhere in the massif. We have defined four plutons, the boundaries of which are underlined by more basic rocks at their margins, that are also more anisotropic and more planar in fabric, having been deformed essentially in the magmatic state. The largest pluton, the Colomers unit, is itself made of sub-plutons which probably equate with individual magma batches. These plutons or sub-plutons were coeval as demonstrated by their juxtaposed concentric trajectories of foliations, and also by their magmatic contacts underlined by anisotropy gradients. Their sources and/or chemical evolutions, however, might have been slightly different, as some monzogranites have two micas whereas others carry biotite and scattered hornblende.

This study has provided new insight concerning, at least, the late stages of emplacement of the Maladeta complex, and consequently the Variscan history of the Pyrenees. The magma was emplaced into brittle crust during a tectonic event not fully understood because its kinematic characteristics remain poorly constrained. That event, however, has to reconcile: (i) the probable formation of openings parallel to two main directions, NE–SW and NW–SE in mean trends, which are the dominant magmatic lineations recorded in this study; and (ii) a probable top-to-the-southwest late magmatic compression, responsible for the highly anisotropic strips and for the N–S lineations in the Sant Nicolau corridor, itself linked to high-temperature solid-state deformations. We think that the late tectonic event, again compressional but dextral in sense, which resulted in high strain localization into narrow mylonitic bands, was late Variscan in age.

The structure of the Maladeta granitic complex is therefore that of a polydiapir, in the sense of individual and more or less coeval magma batches forming a coalescence of domes. However, no indication is available on the mode of magma transport from the source. The emplacement of the polydiapir was essentially syntectonic at the end of the Variscan orogeny. The Alpine orogeny, that arguably transported the complex southwards as a block, seems to have imprinted the granite complex only in the form of brittle faults and, possibly, reactivation of earlier shear zones.

Acknowledgements—We thank the Aigüestortes National Park authority who allowed the sampling. The study has benefited from the careful readings of W. E. Stephens while an Associate Professor in Toulouse, from the reviews of A. McCaig and W. Owens, and from discussions with our colleagues from Spain (J. M. Tubia, V. Santana, Bilbao University; and F. Lobato from Salamanca University). We thank E. Ferré, A. Lissaragues and A. Nédélec who participated to the sampling, and A. M. Roquet and C. Cavaré-Hester for technical assistance in the laboratory. The funding was provided by the CNRS-INSU/DBT Program (contribution # 547). This is a contribution of the URA CNRS No. 67 "Mécanismes de Transfert en Géologie".

REFERENCES

Amice, M., Bouchez, J. L., Aranguren, A., Alvarez, F. & Vigneresse, J. L. 1991. El batolito granitico de Cabeza de Araya (Extremadura): comparacion de sus estructuras magmaticas y magneticas. *Bol. Geol. Minero.* **102–3**, 455–471.

Bouchez, J. L., Gleizes, G., Djouadi, T. & Rochette, P. 1990. Microstructure and magnetic susceptibility applied to emplacement kinematics of granites: the example of the Foix pluton (French Pyrenees). *Tectonophysics* **184**, 157–171.

Carreras, J., Julivert, M. & Santanach, P. F. 1980. Hercynian mylonite belts in eastern Pyrenees: an example of shear-zones associated with late folding. *J. Struct. Geol.* **2**, 5–9.

Charlet, J. M. 1968. Etude préliminaire du massif granitique de la Maladeta (Pyrénées centrales espagnoles). *Ann. Soc. géol. Nord, Lille* **88**, 65–75.

Charlet, J. M. 1979. Le massif granitique de la Maladeta (Pyrénées centrales espagnoles), synthèse des données géologiques. *Ann. Soc. géol. Belgique* **102**, 313–323.

Evans, N. 1992. Deformation in the aureole of the Maladeta granodiorite, Spanish Pyrenees: a record of pluton emplacement. 14e Réunion Sciences Terre, Toulouse, Soc. Géol. France éd., 59.

Gleizes, G. & Bouchez, J. L. 1989. Le granite de Mont-Louis (zone axiale des Pyrénées): anisotropie magnétique, structures et microstructures. *C. r. Acad. Sci. Paris, Sér. II* **309**, 1075–1082.

Gleizes, G., Leblanc, D. & Bouchez, J.-L. 1991. Le pluton granitique de Bassiès (Pyrénées ariègeoises: zonation, structure et mise en place. *C. r. Acad. Sci. Paris, Sér. II* **312**, 755–762

Gleizes, G., Leblanc, D. & Bouchez, J.-L. 1992. Zones de cisaillement dans les granites des Pyrénées: témoins d'une méga-transpression dextre fini-hercynienne? 14e Réunion Sciences Terre, Toulouse, Soc. Géol. France éd., 69.

Gleizes, G., Nédélec, A., Bouchez, J.-L., Autran, A. & Rochette, P. In press. Magnetic susceptibility of the Mont Louis-Andorra ilmenite-type granite (Pyrenees): a new tool for the petrographic characterization and regional mapping of zoned granite plutons. *J. geophys. Res.*

Guillet, P., Bouchez, J. L. & Wagner, J. J. 1983. Anisotropy of magnetic susceptibility and magnetic structures in the Guérande granite massif (France). *Tectonics* **2**, 419–429.

Hrouda, F. 1986. The effect of quartz on the magnetic anisotropy of quartzite. *Studia Geophys. Geod.* **30**, 39–45.

Ildefonse, B. & Fernandez, A. 1988. Influence of the concentration of rigid markers in a viscous medium on the production of preferred orientations. An experimental contribution: non coaxial strain. *Bull. Geol. Inst. Univ. Uppsala* **14**, 55–60.

Ildefonse, B., Launeau, P., Bouchez, J.-L. & Fernandez, A. 1992. Effect of mechanical interactions on the development of shape preferred orientations: a two-dimensional experimental approach. *J. Struct. Geol.* **14**, 73–83.

Ishihara, S. 1977. The magnetite series and ilmenite series. *Mining Geol.* **27**, 293–305.

King, R. F. 1966. The magnetic fabric of some Irish granites. *Geol. J.* **5**, 43–66.

Kleinsmiede, W. F. 1960. Geology of the Valley de Aran (central Pyrenees). *Leidse Geol. Med.* **25**, 129–247.

Lamouroux, C. 1991. Les mylonites des Pyrénées: classification, mode de formation, évolution. *Mém. Soc. géol. Nord, Lille* **19**.

Lamouroux, C., Soula, J. C., Deramond, J. & Debat, P. 1980. Shear zones in the granodioritic massifs of the Central Pyrenees and the behaviour of these massifs during the Alpine orogenesis. *J. Struct. Geol.* **2**, 49–53.

Launeau, P., Bouchez, J.-L. & Benn, K. 1990. Shape preferred orientation of object populations: automatic analysis of digitized images. *Tectonophysics* **180**, 201–211.

Majoor, F. J. M. 1988. A geochronological study of the axial zone of the central Pyrenees, with emphasis on Variscan events and Alpine resetting. *Lab. Isotopen-Geol. Amsterdam* **6**.

McCaig, A. M. & Miller, J. A. 1986. ^{40}Ar–^{39}Ar age of mylonites along the Mérens fault, central Pyrenees. *Tectonophysics* **129**, 149–172.

Pouget, P., Lamouroux, C., Dahmani, A., Debat, P., Driouch, Y., Mercier, A., Soula, J. C. & Vezat, R. 1989. Typologie et mode de mise en place des roches magmatiques dans les Pyrénées hercyniennes. *Geol. Rdsch.* **78**, 537–554.

Rochette, P. 1987. Magnetic susceptibility of the rock matrix related to magnetic fabric studies. *J. Struct. Geol.* **9**, 1015–1020.

Rochette, P., Jackson, M. & Aubourg, C. 1992. Rock magnetism and the interpretation of anisotropy of magnetic susceptibility. *Rev. Geophys.* **30**, 209–226.

Rousset, R. & Daly, L. 1969. Sur la cohérence de la foliation magnétique du granite porphyroïde d'Egletons (Corrèze). *C. r. Acad. Sci. Paris, Sér. D* **268**, 1912–1915.

Soliva, J., Brunel, M. & Matte, P. 1991. La zone de décrochement ductile Le Boulou–Le Perthus dans la granodiorite de Saint-Laurent (Pyrénées orientales). *C. r. Acad. Sci. Paris, Sér. II* **312**, 639–646.

Vitrac-Michard, A., Albarede, F., Dupuis, C. & Taylor, H. P. 1980. The genesis of Variscan (Hercynian) plutonic rocks: inferences from Sr, Pb and O studies on the Maladeta igneous complex, Central Pyrenees (Spain). *Contr. Miner. Petrol.* **72**, 57–72.